Research Paper

Journal of Vascular Research

J Vasc Res 2009;46:218–228
DOI: 10.1159/000165380

Received: February 2, 2008
Accepted after revision: April 12, 2008
Published online: October 27, 2008

Styrene Maleic Acid-Pirarubicin Disrupts Tumor Microcirculation and Enhances the Permeability of Colorectal Liver Metastases

Jurstine Daruwalla[a] Khaled Greish[b] Cathy Malcontenti-Wilson[a]
Vijayaragavan Muralidharan[a] Arun Iyer[c] Hiroshi Maeda[c] Chris Christophi[a]

[a]Department of Surgery, University of Melbourne, Austin Health, Heidelberg, Vic., Australia;
[b]Department of Pharmaceutics and Pharmaceutical Chemistry, University of Utah, Salt Lake City, Utah, USA;
[c]Laboratory of Microbiology and Oncology, Faculty of Pharmaceutical Sciences, Sojo University, Kumamoto, Japan

Key Words
Styrene maleic acid co-polymer · Pirarubicin · Tumor microcirculation · Colorectal cancer · Liver metastases · Doxorubicin · CD34 · Permeability · EPR effect

Abstract
Background: Doxorubicin is a commonly used chemotherapy limited by cardiotoxicity. Pirarubicin, derived from doxorubicin, selectively targets tumors when encapsulated in styrene maleic acid (SMA), forming the macromolecular SMA pirarubicin. Selective targeting is achieved because of the enhanced permeability and retention (EPR) effect. SMA-pirarubicin inhibits the growth of colorectal liver metastases, but tumor destruction is incomplete. The role played by the tumor microcirculation is uncertain. This study investigates the pattern of microcirculatory changes following SMA-pirarubicin treatment. ***Methods:*** Liver metastases were induced in CBA mice using a murine-derived colon cancer line. SMA-pirarubicin (100 mg/kg total dose) was administered intravenously in 3 separate doses. Twenty-four hours after chemotherapy, the tumor microvasculature was examined using CD34 immunohistochemistry and scanning electron microscopy. Tumor perfusion and permeability were assessed using confocal in vivo microscopy and the Evans blue method. ***Results:*** SMA-pirarubicin reduced the microvascular index by 40%. Vascular occlusion and necrosis were extensive following treatment. Viable cells were arranged around tumor vessels. Tumor permeability was also increased. ***Conclusion:*** SMA-pirarubicin damages tumor cells and the tumor microvasculature and enhances tumor vessel permeability. However, tumor necrosis is incomplete, and the growth of residual cells is sustained by a microvascular network. Combined therapy with a vascular targeting agent may affect residual cells, allowing more extensive destruction of tumors.

Introduction

Doxorubicin, a commonly used chemotherapeutic agent, destroys tumors via several mechanisms, one of which involves the production of reactive oxygen species (ROS). However, nonselective accumulation of ROS leads to dose-limiting side effects such as cardiotoxicity [1, 2]. Selective delivery of doxorubicin to tumors reduces side effects, thus allowing the administration of higher doses.

KARGER

Fax +41 61 306 12 34
E-Mail karger@karger.ch
www.karger.com

1018–1172/09/0463–0218$26.00/0

Accessible online at:
www.karger.com/jvr

Dr. Jurstine Daruwalla
Department of Surgery, University of Melbourne
Austin Hospital, Level 8, Lance Townsend Building
Studley Road, Heidelberg, Vic. 3084 (Australia)
Tel. +61 3 9496 5967, Fax +61 3 9458 1650, E-Mail jurstine@pgrad.unimelb.edu.au

Targeted delivery is achieved by exploiting the inherent differences between tumor vasculature and normal vasculature. Compared to normal vessels, tumor vessels exhibit enhanced permeability and retention (EPR) [3]. This phenomenon allows macromolecular drug conjugates (>40 kDa) to selectively leak out of hyperpermeable tumor vessels and remain confined to the tumor interstitium. Most chemotherapeutic agents have a low molecular weight (e.g. 580 Da for doxorubicin) and are indiscriminately delivered to both tumor and normal tissue. We conjugated pirarubicin (627 Da), a derivative of the anthracycline doxorubicin, to styrene maleic acid (SMA) to form SMA-pirarubicin macromolecular micelles (34 kDa). In vivo, SMA-pirarubicin binds to albumin and achieves a molecular weight of 94 kDa, thus allowing it to selectively accumulate in tumors [4]. Using a previously established murine model of colorectal cancer liver metastases [5], we have shown that higher doses of the free drug can be administered in the macromolecular form without toxicity [6]. Despite causing significant tumor destruction, however, necrosis is heterogenous and incomplete [6]. An intact blood supply is essential for the growth and metastasis of tumors [7]. However, there is limited evidence for the direct effect of chemotherapy on the tumor microcirculation. This study investigates changes in the tumor microcirculation using scanning electron and confocal in vivo microscopy as well as changes in vessel architecture, blood flow and permeability. We hypothesize that residual tumor cells following chemotherapy are sustained by a dense microvascular network which ultimately contributes to tumor recurrence.

Methods

Experimental Groups and Drug Administration

Six- to 8-week-old male CBA mice (Laboratory Animal Services, University of Adelaide, S.A., Australia) were housed in standard cages with access to food and water ad libitum. All procedures were performed with approval from the Austin Hospital animal ethics committee. Pirarubicin and SMA-pirarubicin were prepared as described previously [4] and supplied in powder form (Biodynamics Research Foundation, Kumamoto, Japan). The SMA-pirarubicin powder, containing 43% free pirarubicin equivalent, was injected in 0.2 ml of sterile saline. Drugs were administered 14 days after tumor induction. SMA-pirarubicin, 100 mg/kg, was administered via the tail vein (100 mg/kg in total over three divided doses on days 14, 16 and 18 post-tumor induction). Control animals received 0.2-ml saline injections via the tail vein. Free pirarubicin was administered by the same dosing regimen at 10 mg/kg. All assessments were performed 24 h after the final drug dose.

Liver Metastasis Model

Liver metastases were induced using a murine-derived dimethylhydrazine-induced primary colon carcinoma cell line. This model of liver metastases was established previously [5]. The cell line was maintained as solid tumors in the flanks of CBA mice. At the time of induction, tumors were excised and a cell suspension was prepared as previously described [5]. Trypan blue exclusion was used to attain a cell concentration of 1×10^6 cells/ml. Mice were anesthetized using a mixture of ketamine (100 mg/kg; Pfizer, New Zealand) and xylazine (10 mg/kg; Troy Laboratories, Australia). Liver metastases were induced via a 0.05-ml intrasplenic injection (50,000 cells). In this model, macroscopic liver tumors are evident by day 10 following induction. This is followed by a rapid exponential growth phase with the appearance of fully established tumors by day 16 [5].

Microvascular Architecture

Microvascular resin casting was performed to observe changes in the microvascular architecture according to previously described techniques [8]. Briefly, the aorta was cannulated using a 23-gauge intravenous catheter, and the vasculature was perfused with warm saline (120 mm Hg) containing heparin (10 U/ml; Weddell Pharmaceuticals, Sydney, Australia), papaverine (12 mg/ml; David Bull Laboratories, Melbourne, Australia) and 6% polyvinylpyrrolidone (PVP40; Sigma-Aldrich, Melbourne, Australia). Following exsanguination, the vasculature was perfused with a mixture of 10 ml of Mercox blue CL-2B (Okenshoji Co., Tokyo, Japan) and 3.4 ml of methyl methacrylate (Sigma Chemical Co., St. Louis, Mo., USA) with 0.5 ml of a catalyst. The resin was left to polymerize overnight, after which samples were excised and the surrounding tissue digested in 20% potassium hydroxide solution at room temperature. Casts were viewed using scanning electron microscopy (Philips XL30 field emission scanning electron microscope, School of Botany, University of Melbourne, Australia). The tumor microvessel index (total tumor area occupied by microvessels/total tumor area × 100) was calculated using image analysis software (Image-Pro Plus version 4.5, Media Cybernetics) to attain a mean percentage vascular index. Two groups were studied, i.e. control (n = 8) and SMA-pirarubicin-treated mice (n = 8), counting at least 5 tumors per liver.

Tumor Permeability following Administration of SMA-Pirarubicin

Twenty-four hours following the final dose of SMA-pirarubicin, mice were injected with 0.2 ml of Evans blue (Sigma-Aldrich, Sydney, N.S.W., Australia) at a dose of 30 mg/kg via the tail vein. Sixty minutes after injection, mice were transcardially perfused (with 50 ml of saline at 80 mm Hg for 2 min at 37°C) to remove any excess Evans blue that had not absorbed into tissue. Biopsies of tumor and normal liver were excised and placed in formamide (100 mg of tissue/ml of formamide). Tissues were homogenized and incubated at 60°C for 48 h to allow dye extraction. Following incubation and centrifugation (12,000 *g* for 20 min), the supernatant was analyzed using spectrophotometry (Varian Bio UV-100 visible spectrophotometer; Varian, Mulgrave, Vic., Australia) at a wavelength of 620 nm. Four groups were studied: (1) the control group, i.e. liver of non-tumor-bearing mice (n = 10); (2) surrounding liver (of tumor-bearing mice) and tumor (n = 10); (3) SMA-pirarubicin-treated (100 mg/kg) surrounding liver and tumor (n = 10), and (4) free-pirarubicin-treated (MTD 10 mg/kg) sur-

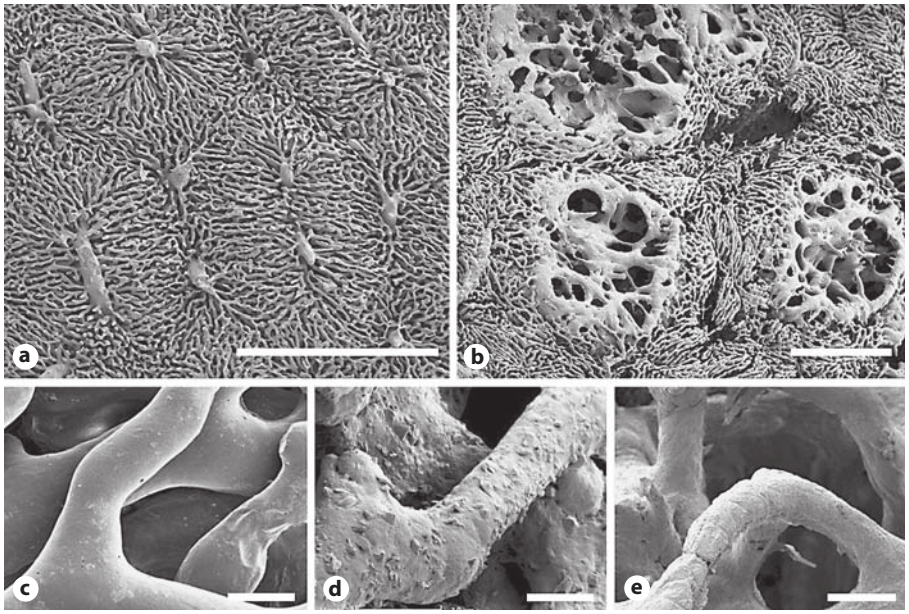

Fig. 1. Scanning electron micrographs of the parenchyma of aplastic versus neoplastic liver sinusoids. **a** Normal liver sinusoids are uniform in pattern, showing demarcation of hepatic lobules. **b** Normal liver of tumor-bearing specimens is invaded by micrometastases which displace the parenchyma, causing distortion of the structured sinusoidal network. **c** Normal liver (naïve) sinusoids at high magnification are smooth with minimal leakiness. **d** Sinusoids in tumor-bearing specimens are leaky. Rough bleb-like projections at the vascular surface are indicative of resin leakage. **e** The normal liver of SMA-pirarubicin-treated specimens displays reduced leakage and resembles naïve sinusoids. Scale bars = 500 μm (**a**, **b**) and 10 μm (**c–e**).

rounding liver and tumor (n = 10). The amount of Evans blue (micrograms per gram) was calculated from standard solutions to determine the concentration of extravasated dye in the tissue.

Assessing Real-Time Changes in Microcirculatory Patterns Using in vivo Confocal Microscopy

The effect of SMA-pirarubicin on tumor and normal liver microcirculation was assessed using confocal in vivo microscopy, which was performed 24 h after drug treatment. Mice were anesthetized and a laparotomy was then performed to expose the liver. An intravenous injection of fluorescein isothiocyanate-dextran (0.05 ml, molecular weight 160 kDa; Sigma-Aldrich, Australia) was administered and mice were placed on a viewing stage and examined under an Olympus BH-2 microscope (Olympus, Australia) connected to a Five 1 confocal system (Optiscan, Melbourne, Australia). Both tumors and normal liver were viewed over a period of 20 min. Still images were captured at different time points to demonstrate alterations in blood flow and extravasation of the fluorescent dextran.

Tumor Necrosis

Tumor histology was observed using hematoxylin and eosin (HE) staining with a standard protocol [9]. Serial sections were examined using light microscopy to detect changes in tumor cell morphology, necrosis and any tumor vessel changes caused by drug therapy.

CD34 Immunohistochemistry

The effect of SMA-pirarubicin on vascular endothelial cells was investigated by immunohistochemistry of paraffin-embedded sections with the commercially available monoclonal rat antimouse CD34 antibody (MCA1825GA; AbD Serotec, New Zealand). Detection was conducted using the Envision+ horseradish peroxidase detection system (K4011; Dako Cytomation, Denmark). Endogenous peroxidase activity was firstly quenched using a peroxidase block (Dako Envision+ kit, K4011; Dako Cytomation). Antigen retrieval was performed using citrate buffer (1 mM, pH = 6) at 99°C for 20 min. Sections were incubated with the primary antibody (1:500) for 2 h at room temperature. The secondary antibody, a polyclonal rabbit antirat antibody (E0468), was applied at a 1:100 dilution for 30 min. Following incubation with horseradish peroxidase complex for 30 min, sections were incubated with diaminobenzidine substrate/chromogen for 10 min. Sections were counterstained with hematoxylin, dehydrated in ascending ethanol and mounted for viewing by light microscopy.

Endothelial cells stained brown. The number of CD34-positive vessels per square millimeter of tumor tissue examined was calculated to attain a vascular index measurement. This was compared with serial HE sections to correlate areas of viable tumor cells. At least 10 tumors were quantified per liver in each treatment group (n = 10).

Statistical Analysis

All data are represented as the mean ± standard error of the mean (SEM). Statistical analysis was conducted using SPSS (Statistical Package for the Social Sciences™, version 10, Chicago, Ill., USA) and ANOVA (followed by Tukey's multiple-comparison test). Pairwise comparisons were analyzed using parametric (Student's t test) or nonparametric (Mann-Whitney) tests where appropriate. All tests were two-sided, and $p < 0.05$ was considered statistically significant. Animal numbers were based on pilot studies, from which we estimated a minimum requirement of 8–10 animals per study group to detect a 20–30% reduction in tumor vessel index and a 10–20% change in permeability, each with a power of at least 0.8.

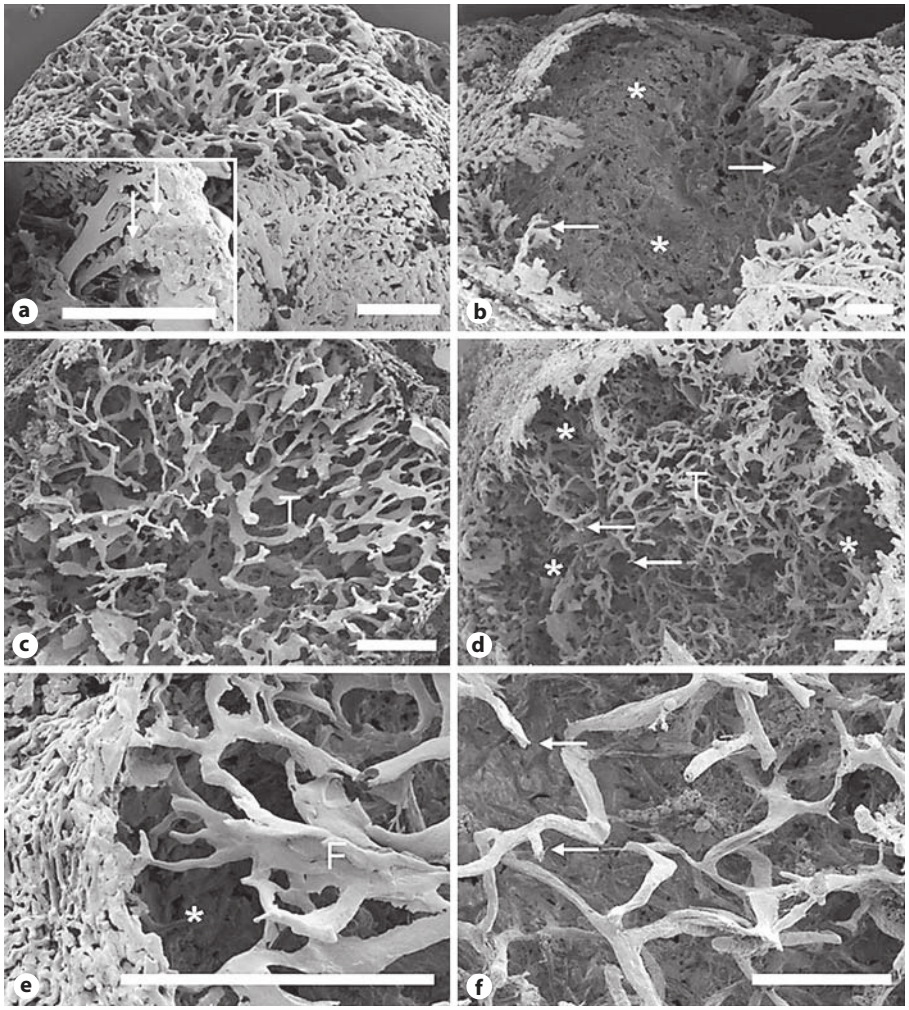

Fig. 2. SMA-pirarubicin destroys the tumor microvascular network. **a**, **c**, **e** Control tumors exhibit a highly aberrant microvasculature (T) with dilated and flattened vessels (F). Vessels are continuous at the interface, consistent with sinusoid-derived angiogenesis (**a**, inset, arrows). **b**, **d**, **f** Tapered ends (arrows) leading to filling defects were more common amongst SMA-pirarubicin-treated tumors compared to control tumors. This was suggestive of necrosis (**b**, **d**, **e**, *). **e**, **f** Differences in the microvessel index and vessel diameter were apparent at high power between control and treated tumors. Control tumors had numerous flattened (F) vessels. Treated tumors exhibited fewer and narrower tumor vessels. Scale bars = 500 μm.

Results

Effect of SMA-Pirarubicin on Tumor Microvascular Architecture

Alterations in the vascular architecture were assessed 24 h after the last dose of SMA-pirarubicin. Two different comparisons were made: between the liver sinusoids of mice with and without (naïve) tumors (fig. 1) and between tumor-bearing mice with and without drug treatment (fig. 2). Scanning electron micrographs of normal liver demonstrate a highly organized microvascular structure with sinusoids of regular shape and size (fig. 1a). No major filling defects were observed and there was minimal sinusoidal leakage of resin. Normal liver of tumor-bearing mice had micrometastases distributed throughout the parenchyma, creating distortion of the sinusoidal network (fig. 1b). At high magnification, normal liver sinusoids were smooth, demonstrating minimal leakiness (fig. 1c). Sinusoids in tumor-bearing specimens, however, were leaky, with bleb-like projections on the vessel surface (fig. 1d). The sinusoids of SMA-pirarubicin-treated specimens had fewer blebs on the vessel surface and more closely resembled naïve (non-tumor-bearing) sinusoids (fig. 1c vs. e).

The vasculature of control tumors was highly dense and disorganized, with vessels of varying length and diameter. There was evidence of sinusoid-derived angiogenesis indicated by vascular continuity at the tumor-host interface (fig. 2a, inset). Tumor vessels arising from the periphery were dilated and flattened, forming vascular lakes of coalesced vessels (fig. 2a, c). Twenty-four hours after the final dose of SMA-pirarubicin, microvessels were fewer and shorter in length. Tumor vessels were discontinuous and tapered towards regions of complete vascular occlusion immediately beyond the tumor periphery (fig. 2b, d). This gave rise to large filling defects

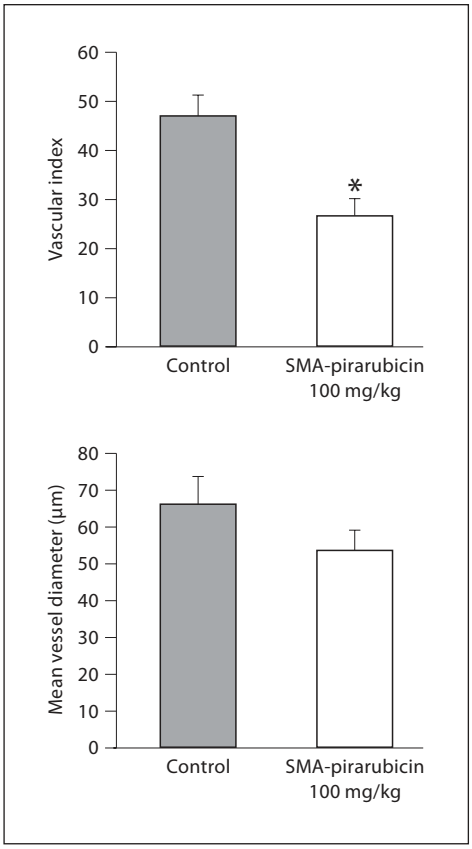

Fig. 3. Changes in the microvascular index following SMA-pirarubicin treatment after 24 hours. The microvascular index was calculated for each tumor (area occupied by patent vessels/total area of tumor × 100). SMA-pirarubicin reduced the tumor microvascular index by 40% (27 ± 3.7% vs. control, 47 ± 4.4%; p = 0.003, Mann-Whitney test). The mean vessel diameter was reduced, but this was not statistically significant (54 ± 5.5 μm vs. control, 66 ± 7.3 μm; p = 0.3, Mann-Whitney test). Bars indicate means ± SEM. * $p < 0.005$: significant difference versus control.

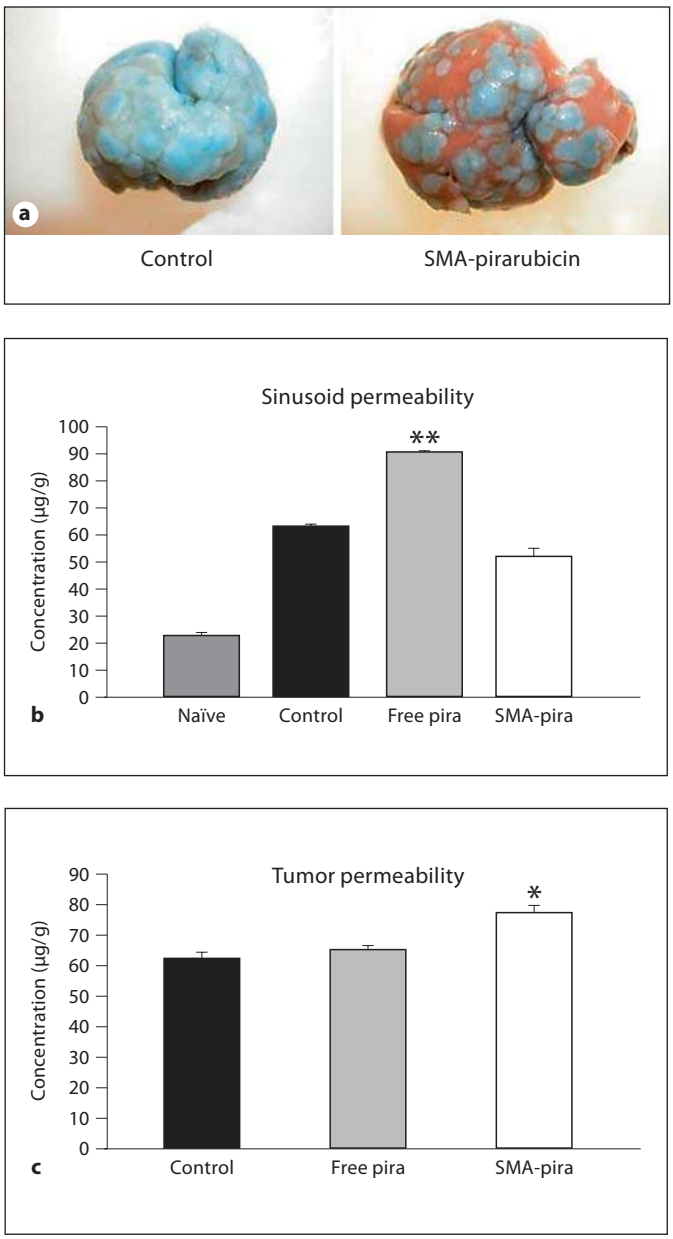

Fig. 4. Changes in permeability following treatment with SMA-pirarubicin and free pirarubicin. **a** Normal liver of control specimens retained more dye compared to the normal liver of treated specimens. **b** Normal liver sinusoids of non-tumor-bearing specimens (naïve) demonstrated minimal permeability. Sinusoids of tumor-bearing specimens exhibited enhanced permeability (although not statistically significant). Free pirarubicin significantly increased sinusoidal permeability. **c** Tumor vessel permeability was significantly increased with SMA-pirarubicin treatment compared to untreated and free-pirarubicin-treated tumors. Bars indicate means ± SEM. * $p < 0.05$, ** $p < 0.005$: significant differences versus control (ANOVA using Tukey's method).

identified as an absence of vessels or regions of necrosis. SMA-pirarubicin significantly reduced the tumor microvascular index (fig. 3) to 26.5 ± 3.7% compared to the control group (46.8 ± 4.4%; p = 0.003, Mann-Whitney test). Mean tumor vessel diameter decreased from 66.27 ± 7.26 μm in controls to 53.64 ± 5.46 μm in drug-treated animals; however, this was not statistically significant (p = 0.291, Mann-Whitney test).

Altered Tumor Permeability following Administration of SMA-Pirarubicin

Changes in vascular permeability following administration of SMA-pirarubicin and free pirarubicin were as-

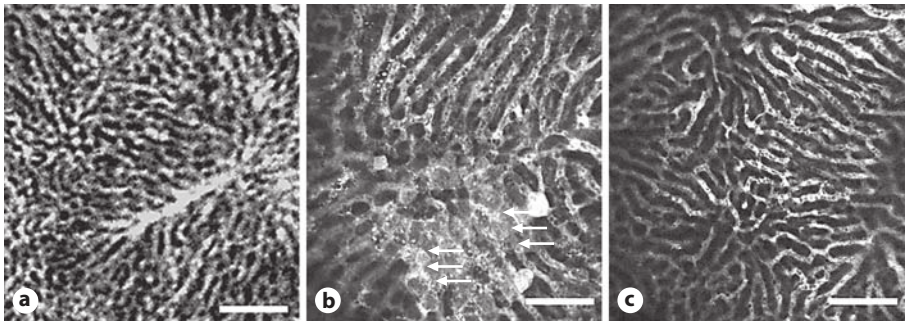

Fig. 5. Changes in the microcirculation of normal liver following SMA-pirarubicin treatment. **a** Normal liver (non-tumor-bearing specimens) shows the sinusoidal network. This is distorted in control (tumor-bearing) specimens. **b** There is increased perisinusoidal extravasation of dextran after injection in control (tumor-bearing) specimens (arrows). **c** Normal liver of SMA-pirarubicin-treated specimens closely resembled the parenchyma of non-tumor-bearing specimens, with minimal sinusoidal leakage. Scale bars = 500 μm.

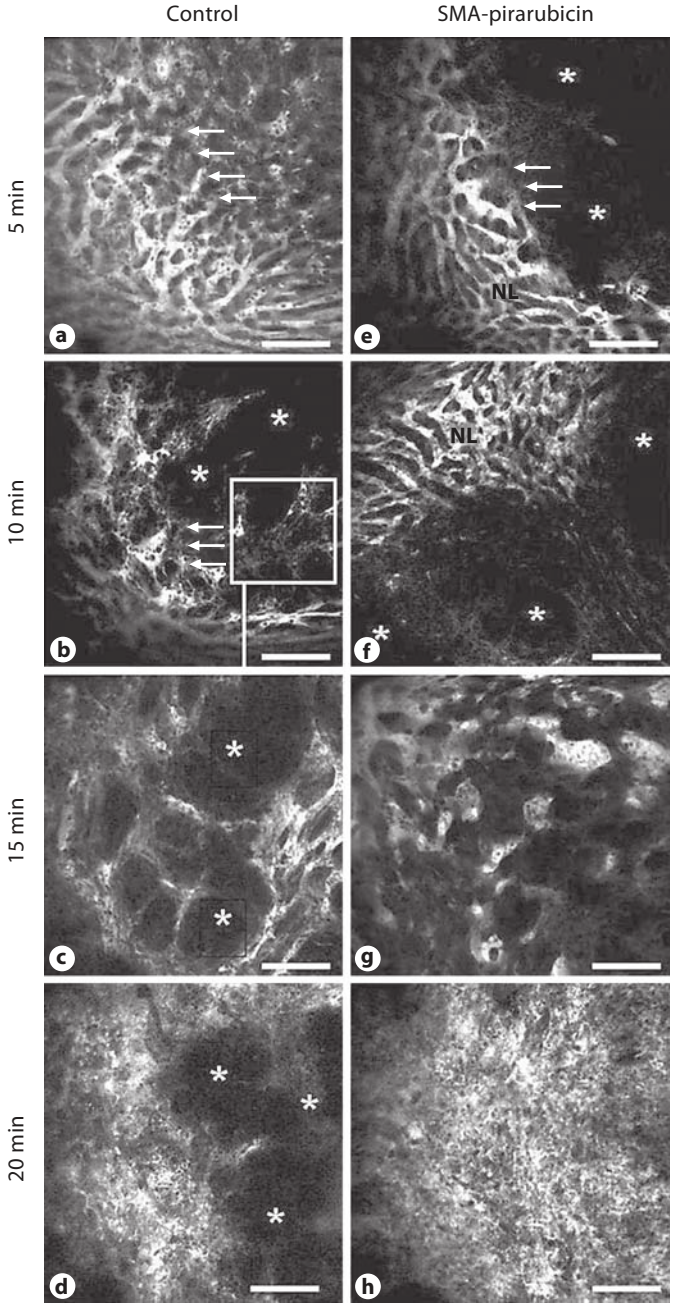

Fig. 6. Changes in tumor microcirculation following SMA-pirarubicin treatment. **a** There was substantial extravasation of dextran at the tumor-host interface (arrows) of control tumors. **b**, **c** Large quantities of dextran diffused into the tumor over the next 10–15 min, indicative of the EPR effect and demonstrating the dense microvascular network of untreated tumors. Outlines of the vessel walls can be seen, interspersed with regions of an absence of filling (*). **d** Further extravasation at 20 min showed leakage of dextran from these vessels but the unfilled regions persisted (*). This suggests that these regions were filled by tumor cells. **e**, **f** Little extravasation of dextran was observed at the tumor-host interface of SMA-pirarubicin-treated tumors (arrows). **f**, **g** After 10–15 min, dextran had extravasated further into the tumor. Again regions of an absence of filling were observed (*). Two characteristics were unique to and consistent amongst treated tumors: firstly, clusters of dextran were commonly observed within the tumor (**g**) and, secondly, after 20 min, dextran showed diffuse extravasation across entire regions within the tumor without any absence of filling, indicating that these regions are void of tumor cells (**h**). Scale bars = 500 μm.

sessed 24 h after the final drug dose. All values are represented as the concentration of Evans blue dye (micrograms per gram of tissue) extravasated from vessels into tissues. Following drug treatment, changes in permeability were observed in the sinusoids as well as the tumor vessels. Sinusoids of normal liver without tumors (naïve sinusoids) demonstrated minimal permeability. Sinusoidal permeability was significantly increased in tumor-bearing (control) specimens and free-pirarubicin-treated samples (90.8 ± 0.3 μg/g compared to 23 ± 0.8 μg/g in naïve sinusoids; p = 0.003, ANOVA using Tukey's method; fig. 4b). SMA-pirarubicin-treated sinusoids had reduced permeability compared to control sinusoids (51.9 ± 3.0 μg/g vs. control, 63 ± 0.9 μg/g). Tumor vessels treated with SMA-pirarubicin had significantly enhanced permeability compared to untreated tumor vessels (77.5 ± 2.5 μg/g vs. control, 62.5 ± 2.0 μg/g; p = 0.03, ANOVA using Tukey's method; fig. 4c). Treatment with free pirarubicin significantly increased sinusoidal permeability but did not alter tumor vessel permeability.

Assessing Real-Time Changes in Microcirculation Using Confocal in vivo Microscopy

Microcirculatory changes 24 h after SMA-pirarubicin treatment were visualized by intravital laser confocal microscopy. Mice were injected with fluorescent dextran and observed over 20 min. Leakage of the dextran is suggestive of increased vascular permeability, which may be due to vessel damage or the inherent leakiness of tumor vessels. Following administration of the fluorescent dye, naïve liver sinusoids (non-tumor-bearing livers) exhibited maximum and homogenous fluorescence intensity with minimal dye leakage (fig. 5a). Sinusoids of control (tumor-bearing) specimens exhibited substantial extravasation of dextran into the perisinusoidal space (fig. 5b, arrows). Following drug treatment, sinusoidal leakage was reduced and resembled naïve sinusoids (fig. 5c).

In control tumors, dextran was observed (over 10–15 min) throughout the dense microvascular network (fig. 6a–d). Control tumor vasculature was interspersed with regions of an absence of fluorescence. After 20 min, these regions remained unfilled, suggesting that they were occupied by tumor cells (fig. 6d). The microcirculation of SMA-pirarubicin-treated tumors showed altered characteristics. In some treated tumors, blood flow was occluded beyond the tumor periphery, leaving a large central area with an absence of filling (fig. 6e, f). In this case, minimal extravasation of dextran was observed at the tumor-host interface (fig. 6e, f, arrows). In other treated tumors, over the next 10–15 min, the dextran had homogenously extravasated throughout these regions (fig. 6g, h), suggesting that these regions were void of tumor cells and most probably necrotic matrices. Another unique feature of treated tumors was the presence of dextran clusters heterogeneously taken up by groups of tumor cells (fig. 6g).

Tumor Necrosis and CD34 Immunohistochemistry

Control tumors were cohesive and moderately differentiated, with minimal central necrosis (fig. 7a). Control tumors demonstrated a high degree of CD34 staining. Vessels were numerous and in close proximity to each other, allowing tumor cells to grow perivascularly (fig. 7b, inset). In contrast, SMA-pirarubicin-treated tumors were smaller and exhibited a high degree of central necrosis, with residual tumor cells restricted to a thin viable rim at the periphery in some tumors (fig. 7c). Overall, treated tumors demonstrated heterogeneous and incomplete necrosis. Some tumors demonstrated extensive central necrosis, with viable cells restricted to the tumor periphery, while other tumors demonstrated patchy necrosis interspersed with viable tumor cells (fig. 7c, inset). A common observation was the close proximity of surviving tumor cells to a vessel (fig. 7d, e, insets). The number of CD34-positive vessels per square millimeter of tissue examined was also quantified, to obtain the vascular index. The vascular index was significantly reduced 24 h after the final drug dose (47.1 ± 0.7% vs. control, 93.6 ± 0.8%, p = 0.03, Mann-Whitney test).

Discussion

Pirarubicin (tetrahydropyranyl-doxorubicin) is a derivative of the anthracycline antibiotic doxorubicin. It intercalates DNA, causing strand breaks, and interferes with DNA replication and repair by inhibiting topoisomerase II [10]. One other main action of pirarubicin is the production of ROS, which are toxic to tumor cells. Pirarubicin has a low molecular weight (0.627 kDa) and is indiscriminately delivered to both tumor and normal tissue, leading to dose-limiting side effects such as cardiotoxicity [1, 2]. Conjugation of pirarubicin to SMA forms macromolecular micelles (34 kDa). In circulation, these micelles bind albumin and attain a final molecular weight of 94 kDa [4]. Molecules larger than 40 kDa selectively leak out of tumor vessels but remain confined to the vascular compartment of normal vessels. We have previously shown that SMA-pirarubicin (50 mg/kg over 3 separate doses) significantly reduces the growth of colorectal liver

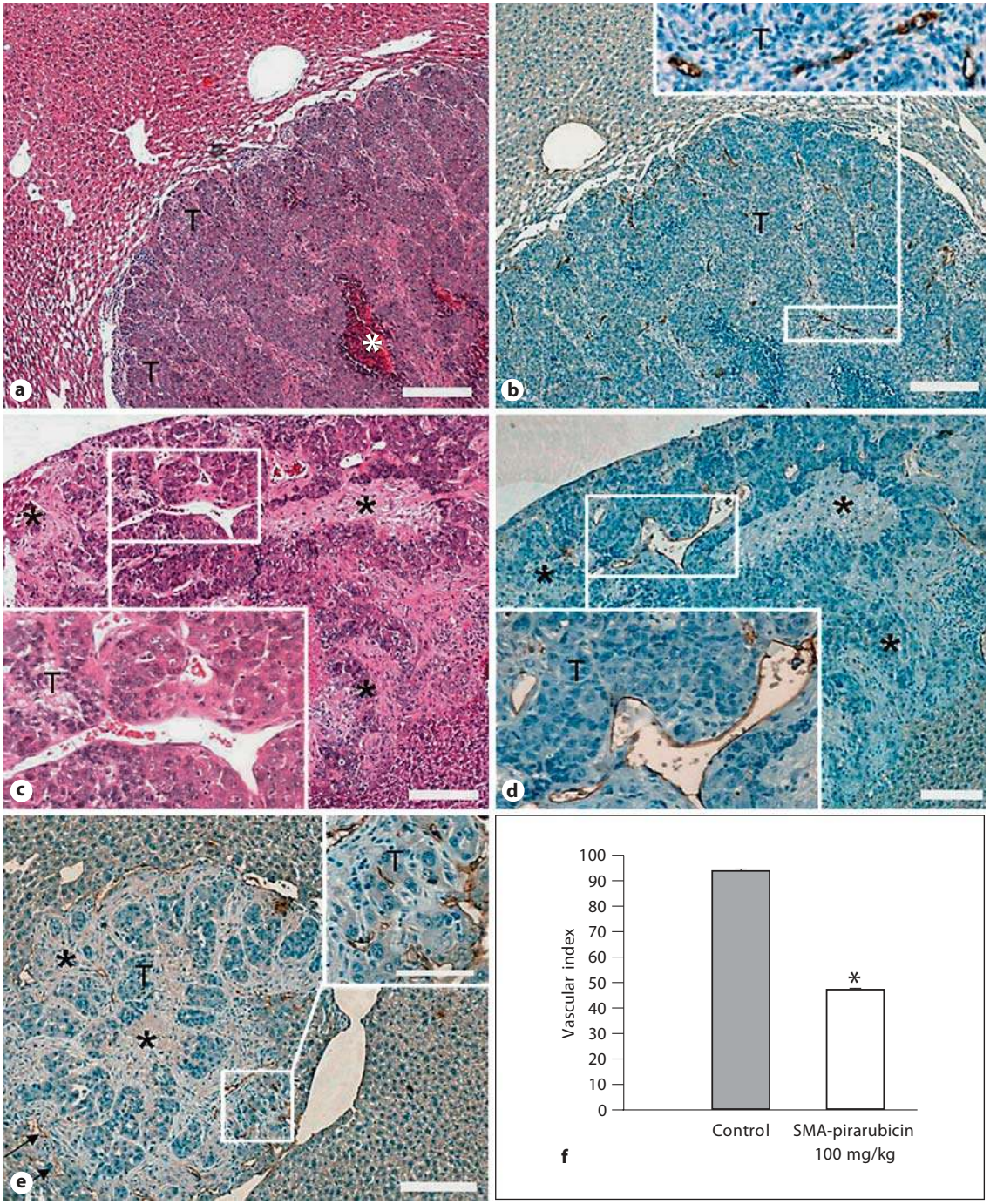

Color version available online

Fig. 7. a–e Viable tumor cells (T) are supplied by tumor blood vessels. Untreated tumors demonstrated minimal central necrosis (**a**, *) and a high degree of CD34 staining. Tumor vessels were arranged close to each other, providing a rich vascular supply to perivascular tumor cells (**b**, inset). SMA-pirarubicin-treated tumors had a high degree of necrosis (*), with residual tumor cells restricted to patches within the tumor or a rim at the periphery (**c**, inset). Surviving tumor cells were in close proximity to tumor vessels (**c**, **d** and **e**, insets). **f** The number of CD34-positive tumor vessels per square millimeter of tumor tissue examined was calculated to determine the vascular index, which was significantly reduced 24 h after the final drug dose (* $p = 0.03$, Mann-Whitney test). Scale bars = 200 μm (**a–e**) and 100 μm (**e**, inset).

metastases. Tumor necrosis, however, is incomplete [6]. Using HE staining, we have shown that only patches of tumor cells survived 24 hours following chemotherapy. In some tumors, these patches are confined to the periphery, while in others, the patches are distributed throughout the tumor. Histologically, these cells appear to be viable and not necrotic or apoptotic. Incomplete necrosis in the form of a viable rim has been reported as a major limitation of drug therapy by other studies [11–13]. Despite the importance of tumor vessels, few studies define the direct effects of chemotherapy on the microcirculation. This study investigated the changes in the microvasculature following SMA-pirarubicin treatment and its role in sustaining tumor growth after chemotherapy.

Our collaborators have developed a more stable formulation of SMA-pirarubicin. Using this new formulation, we established the MTD of SMA-pirarubicin to be 100 mg/kg, without toxicity. We firstly determined changes in tumor vessel ultrastructure following drug treatment, including effects on tumor vessel architecture, permeability and microcirculation.

SMA-pirarubicin (100 mg/kg) had significant effects on the microcirculation of tumors with little effect on normal sinusoids. Sinsusoids of control specimens had an uneven surface with vascular sprouts and bleb-like projections. These were indicative of regions where resin had extravasated from the vessel lumen due to enhanced leakiness. Large intercellular gap junctions are a unique feature of tumor vessels and form the basis for enhanced permeability [3, 14]. SMA-pirarubicin-treated sinusoids appeared smoother and resembled normal (naïve) sinusoids.

SMA-pirarubicin reduced the tumor microvessel index by over 40%, as demonstrated by our scanning electron microscopy (SEM) studies. A similar reduction in the microvessel index following doxorubicin treatment has been reported previously [15]. Following treatment, tumor vessels were shorter, although vessel diameter remained unaltered. Of particular interest from these studies is the number of tapered endings after treatment. Treated tumors demonstrated vessels which ran into the tumor but underwent vascular occlusion before they reached the tumor center, thus forming a tapered end. Vessel occlusion to this extent would undoubtedly reduce tumor blood flow (although this was not directly measured). Unlike vascular targeting agents which cause the death of tumor cells secondary to vascular shutdown, SMA-pirarubicin is not targeted to endothelial cells – although it has demonstrated cytotoxicity against endothelial cells [16, 17]. Our SEM studies showed that there were regions of absent filling after treatment. These regions were void of either vessels or cells. It is possible that SMA-pirarubicin injected intravenously firstly affects tumor endothelial cells and then, once these cells die, the surrounding tumor cells are deprived of nutrients and also die.

We know that pirarubicin intercalates DNA, inhibits the enzyme DNA-topoisomerase and induces lipid peroxidation via ROS production. These processes are toxic to both tumor and endothelial cells. This is also supported by our histological studies, in which necrotic regions were also void of CD34 staining. Morphologically, residual tumor cells appeared enlarged and swollen at high magnification 24 h after drug treatment (data not shown). We therefore conclude that SMA-pirarubicin is cytotoxic to both tumor and endothelial cells.

One of the suggested limitations of liposomal doxorubicin is a lack of penetration into tumors [15, 18]. Our data is in disagreement with this, since SMA-pirarubicin caused marked central necrosis in many tumors. The limiting factor in this case was incomplete and heterogeneous necrosis. Some studies have proposed that residual cells are supplied by oxygen and nutrients diffusing from the surrounding normal tissue. Although we accept that diffusion plays a part, our findings demonstrate that after chemotherapy, tumor cells survive in patchy regions not only at the tumor periphery but also at the center of some tumors. Our CD34 studies show that these tumor cells are in close proximity to tumor vessels. This raises the question of why these cells are not being destroyed. The problem may not be a lack of drug delivery but rather a lack of perfusion of tumor tissue.

Drug delivery is limited by two physiological parameters. Firstly, interstitial pressure within tumors is elevated due to constant extravasation from hyperpermeable vessels coupled with defective lymphatic drainage [19–21]. However, vessel hyperpermeability and tortuosity induce stasis of the blood flow. This creates a low-pressure gradient which ultimately limits the extravasation of macromolecules despite enhanced permeability. Secondly, the rapidly growing population of tumor cells puts pressure on the newly established vasculature, causing vascular collapse and occlusion [19]. This is supported by our microvascular casts, which demonstrated dilated and flattened vessels at the tumor periphery.

Using the Evans blue method, we showed enhanced sinusoidal permeability in livers containing tumors compared to naïve liver sinusoids. This is due to the induction of vascular endothelial growth factor, which we have shown to be upregulated in normal liver following the induction of tumors [9]. Sinusoidal leakage is a sign of endothelial damage, as the tight junctions between ad-

jacent endothelial cells are disrupted. There was a significant increase in sinusoidal permeability following treatment with free pirarubicin (10 mg/kg). SMA-pirarubicin, however, did not cause increased sinusoidal permeability. In fact, sinusoidal permeability was substantially reduced following drug treatment and was similar to that of naïve (non-tumor-bearing) sinusoids This further demonstrates that SMA-pirarubicin selectivley accumulates in tumors with minimal damage to normal tissue.

In this study, SMA-pirarubicin was administered at 48-hour intervals, given our previous findings that intratumoral drug levels diminish after 48 h [4]. Using the Evans blue method, we showed increased tumor permeability 24 h after the final dose of SMA-pirarubicin. This drug-induced permeability could facilitate further extravasation of another dose administered at 24 h instead of 48 h.

Confocal in vivo microscopy demonstrated that vessels of control tumors were intact and ran towards the tumor center with minimal leakage. Reduced leakage is due to the presence of tumor cells in perivascular regions, which limits the space into which the dextran can diffuse. Diffusion from control tumor vessels was restricted in this way. In treated tumors, however, the dextran diffused over a larger area after 20 minutes, indicating an absence of tumor cells in these regions. Another characteristic of treated tumors was the presence of clusters of dextran taken up by surrounding tumor cells, which most likely indicates compromised membrane integrity due to cytotoxic damage in these cells.

Our results show that SMA-pirarubicin induces substantial damage at the tumor site due to selective macromolecular delivery by the EPR effect, which had a direct effect on tumor vessels. Microvascular destruction is to some degree due to endothelial cell destruction, but not entirely, as many vessels undergo vascular shutdown. The main findings of the present study demonstrate that residual cells after chemotherapy are supplied by a rich microvascular network. This network is occluded beyond the tumor periphery in most tumors. The absence of vasculature beyond this point is synonymous with regions of necrosis due to the cytotoxicity of the drug. As for residual tumor cells, whether drug delivery is compromised or whether they are resistant remains to be identified. Nevertheless, the ability of SMA-pirarubicin to induce vascular destruction provides a rationale for the administration of an additional antivascular drug to achieve an additive effect or the possibility of combination with an antiangiogenic agent in an effort to normalize the vasculature and thereby enhance drug delivery. Further studies beyond 24 hours and intermittent administration of SMA-pirarubicin at the same or higher doses may achieve a more definite conclusion.

Acknowledgements

We would like to thank Dr. Simon Crawford (School of Botany, University of Melbourne, Australia) and Dr. Wendy McLaren (Optiscan, Victoria, Australia) for their expertise and technical assistance.

This work was supported by the National Health and Medical Research Council grant No. 400190.

References

1 Hirano S, Wakazono K, Agata N, Iguchi H, Tone H: Comparison of cardiotoxicity of pirarubicin, epirubicin and doxorubicin in the rat. Drugs Exp Clin Res 1994;20:153–160.

2 Zhou S, Palmeira CM, Wallace KB: Doxorubicin-induced persistent oxidative stress to cardiac myocytes. Toxicol Lett 2001;121:151–157.

3 Maeda H, Wu J, Sawa T, Matsumura Y, Hori K: Tumor vascular permeability and the EPR effect in macromolecular therapeutics: a review. J Control Release 2000;65:271–284.

4 Greish K, Sawa T, Fang J, Akaike T, Maeda H: SMA-doxorubicin, a new polymeric micellar drug for effective targeting to solid tumours. J Control Release 2004;97:219–230.

5 Kuruppu D, Christophi C, Bertram JF, O'Brien PE: Characterization of an animal model of hepatic metastasis. J Gastroenterol Hepatol 1996;11:26–32.

6 Daruwalla J, Greish K, Nikfarjam M, Millar I, Malcontenti-Wilson C, Iyer AK, Christophi C: Evaluation of the effect of SMA-pirarubicin micelles on colorectal cancer liver metastases and of hyperbaric oxygen in CBA mice. J Drug Target 2007;15:487–495.

7 Daruwalla J, Christophi C: Hyperbaric oxygen therapy for malignancy: a review. World J Surg 2006;30:2112–2131.

8 Kuruppu D, Christophi C, Maeda H, O'Brien PE: Changes in the microvascular architecture of colorectal liver metastases following the administration of SMANCS/lipiodol. J Surg Res 2002;103:47–54.

9 Daruwalla J, Nikfarjam M, Malcontenti-Wilson C, Muralidharan V, Christophi C: Effect of thalidomide on colorectal cancer liver metastases in CBA mice. J Surg Oncol 2005;91:134–140.

10 Fornari FA, Randolph JK, Yalowich JC, Ritke MK, Gewirtz DA: Interference by doxorubicin with DNA unwinding in MCF-7 breast tumor cells. Mol Pharmacol 1994;45:649–656.

11 Grosios K, Loadman PM, Swaine DJ, Pettit GR, Bibby MC: Combination chemotherapy with combretastatin A-4 phosphate and 5-fluorouracil in an experimental murine colon adenocarcinoma. Anticancer Res 2000;20:229–233.

12 Blakey DC, Westwood FR, Walker M, Hughes GD, Davis PD, Ashton SE, Ryan AJ: Antitumor activity of the novel vascular targeting agent ZD6126 in a panel of tumor models. Clin Cancer Res 2002;8:1974–1983.
13 Chan LS, Malcontenti-Wilson C, Muralidharan V, Christophi C: Effect of vascular targeting agent Oxi4503 on tumor cell kinetics in a mouse model of colorectal liver metastasis. Anticancer Res 2007;27:2317–2323.
14 Hashizume H, Baluk P, Morikawa S, McLean JW, Thurston G, Roberge S, Jain RK, McDonald DM: Openings between defective endothelial cells explain tumor vessel leakiness. Am J Pathol 2000;156:1363–1380.
15 Chen Q, Tong S, Dewhirst MW, Yuan F: Targeting tumor microvessels using doxorubicin encapsulated in a novel thermosensitive liposome. Mol Cancer Ther 2004;3:1311–1317.
16 Wang S, Kotamraju S, Konorev E, Kalivendi S, Joseph J, Kalyanaraman B: Activation of nuclear factor-κB during doxorubicin-induced apoptosis in endothelial cells and myocytes is pro-apoptotic: the role of hydrogen peroxide. Biochem J 2002;367:729–740.
17 Zhang L, Yu D, Hicklin DJ, Hannay JA, Ellis LM, Pollock RE: Combined anti-fetal liver kinase 1 monoclonal antibody and continuous low-dose doxorubicin inhibits angiogenesis and growth of human soft tissue sarcoma xenografts by induction of endothelial cell apoptosis. Cancer Res 2002;62:2034–2042.
18 Wu NZ, Da D, Rudoll TL, Needham D, Whorton AR, Dewhirst MW: Increased microvascular permeability contributes to preferential accumulation of stealth liposomes in tumor tissue. Cancer Res 1993;53:3765–3770.
19 Padera TP, Stoll BR, Tooredman JB, Capen D, di Tomaso E, Jain RK: Pathology: cancer cells compress intratumour vessels. Nature 2004;427:695.
20 Jain RK: Vascular and interstitial barriers to delivery of therapeutic agents in tumors. Cancer Metastasis Rev 1990;9:253–266.
21 Yuan F, Leunig M, Huang SK, Berk DA, Papahadjopoulos D, Jain RK: Microvascular permeability and interstitial penetration of sterically stabilized (stealth) liposomes in a human tumor xenograft. Cancer Res 1994;54:3352–3356.